JACS
JOURNAL OF THE AMERICAN CHEMICAL SOCIETY
pubs.acs.org/JACS
Communication

Selective Interactions between Free-Atom-like *d*-States in Single-Atom Alloy Catalysts and Near-Frontier Molecular Orbitals

Taylor D. Spivey and Adam Holewinski*

Cite This: *J. Am. Chem. Soc.* 2021, 143, 11897–11902
Read Online
ACCESS | Metrics & More | Article Recommendations | Supporting Information

ABSTRACT: In the limit of dilute alloying—the so-called "single-atom alloy" (SAA) regime—certain bimetallic systems exhibit weak mixing between constituent metal wave functions, resulting in sharp, single-atom-like electronic states localized on the dilute component of the alloy. This work shows that when these sharp states are appropriately positioned relative to given molecular orbitals, selective hybridization is enhanced, in accordance with intuitive principles of molecular orbital theory. We demonstrate the phenomenon for activation pathways of crotonaldehyde, a model α,β-unsaturated aldehyde relevant to a wide range of chemical manufacturing. This analysis suggests new possible strategies for selectivity control in heterogeneous catalysis.

Transition metal surfaces are often poorly selective toward activating specific molecular bonds—for example, in performing partial oxidation or partial hydrogenation on multifunctional molecules.[1,2] High activity with poor selectivity can in part be attributed to a high, but energetically broad density of *d*-states near the Fermi level, leading to facile hybridization with multiple molecular orbitals (MOs) of a substrate.[3,4] Interestingly, in the limit of dilute alloying between transition and noble metals, weak mixing between constituent metal wave functions can result in narrow, "free-atom-like" electronic states.[5,6] Illustrative density functional theory (DFT) calculations[7,8] are shown in Figure 1A, displaying the local, *d*-orbital projected density of states (pDOS) for a surface atom in monometallic Au (host element), and for the same atomic site exchanged for a single atom of Ni or Pt (guest elements). Periodic trends are elaborated in Figure S1.

Previously, a number of SAA systems have been identified to exhibit unique reactivity relative to their monometallic constituents.[9−11] However, this observation has mainly been explained in the context of creating bifunctional surfaces that exploit the reactivity of a dopant while avoiding contiguous ensembles of this reactive element and favoring the selectivity of the nobler host through site coupling. For example, Pd sites on a Cu surface can facilitate H_2 dissociation, while entropy-driven spillover still permits a high availability of hydrogen on Cu sites;[12] this has been translated to practical semi-hydrogenation catalysts for alkynes and dialkenes.[13−17] Direct effects from narrowed electronic states have been suggested in regard to a few reactions,[5,6,18] but such effects have not been characterized in a generalizable way.

It could be expected that such free-atom-like states should—similarly to atomic orbitals—hybridize most strongly with molecular states that are energetically resonant. In some regards this is similar to what is approximated in the well-known *d*-band theory of chemisorption—the *d*-states referred to here as "broad" are still quite localized in comparison to *sp*-states, and they are often considered to behave like atomic

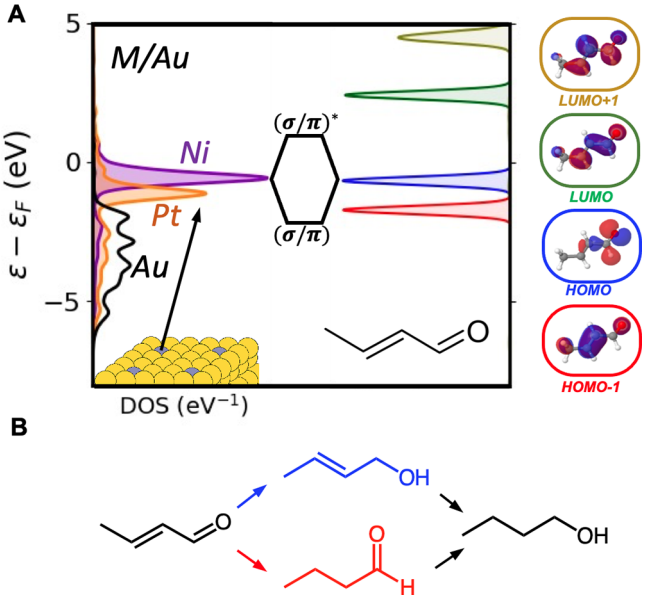

Figure 1. (A) Left: *d*-projected DOS for single-atom-alloys with an Au(111) host. The colored atom of the inset is the substituted site, for which the *d*-pDOS is plotted: Ni (purple), Pt (orange), and unsubstituted Au (black). Right: Frontier and adjacent orbitals for crotonaldehyde. Electron density isosurfaces are outside the plot, which shows corresponding pDOSs at 5 Å from an Au surface. (B) Reduction pathways for crotonaldehyde, related to interactions with the MOs localized on particular functional groups.

Received: April 22, 2021
Published: July 28, 2021

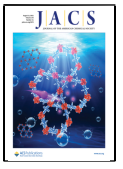

https://doi.org/10.1021/jacs.1c04234
J. Am. Chem. Soc. 2021, 143, 11897−11902

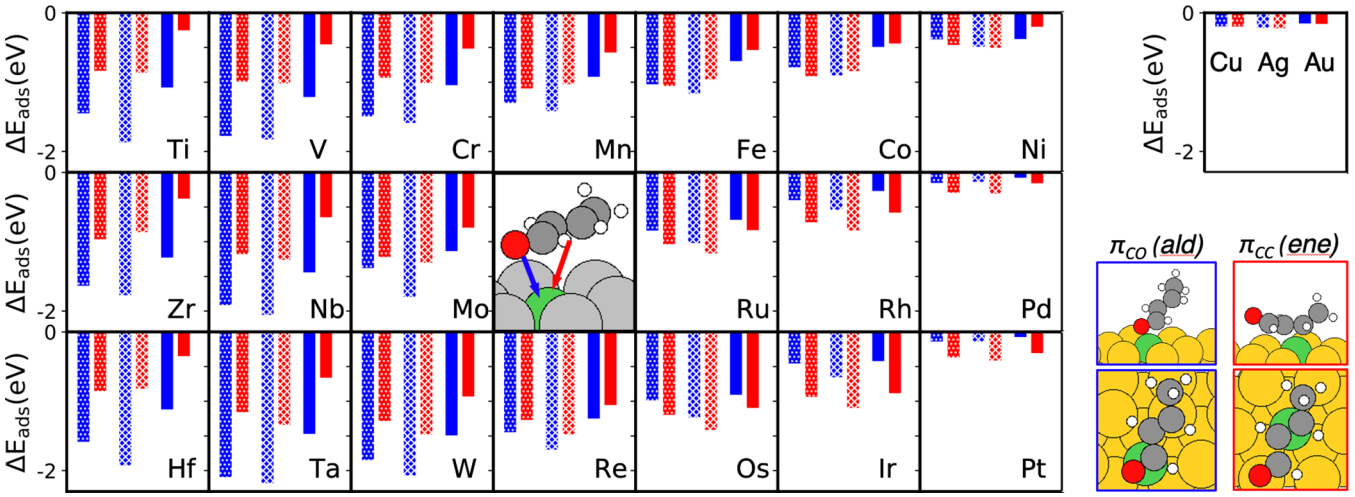

Figure 2. Adsorption enthalpies for crotonaldehyde in each stable geometry (insets) across SAAs. Pairs of hatched bars correspond (left to right) with Cu (dotted), Ag (cross-hatched), and Au (solid) hosts for the respective guest elements. Blue bars signify ald-mode; red, ene-mode.

orbitals in simplified two-level interaction models.[19,20] However, we illustrate here that the extreme localization in so-called "single-atom alloys" (SAAs) amplifies the consequences of this approximation with regard to selective interactions. The concept is schematically shown in Figure 1A, where the pDOS of the SAA systems are shown next to computed MOs of crotonaldehyde (a representative α,β-unsaturated aldehyde[21]), with bonding and antibonding states preferentially forming with a particular MO. The MOs of most interest localize about the aldehyde group (HOMO) and alkene group (HOMO−1), and interaction of catalysts with these states has been suggested to govern periodic selectivity trends in reduction of the respective functional groups toward unsaturated alcohol (more challenging) or saturated aldehyde (Figure 1B).[22] The LUMO is also relevant, but is delocalized and has little influence on trends (Figures S2−S3 and Supporting Methods).

A survey of adsorption preferences of crotonaldehyde on a series of SAA surfaces (transition metals in Cu, Ag, or Au (111) hosts) is summarized in Figure 2. Among possible adsorption geometries,[23] two, corresponding to interactions with either functional group, show energy minima on SAA guest sites. We categorize the pathways as "ene-approach" and "ald-approach" (Figure 2 inset), where the respective geometries are a η^2-π_{CC} configuration atop the guest atom or a π_{CO} mode mainly involving an oxygen lone pair. There is a clear preference for alkene binding on late transition metal sites, while the earlier transition metals prefer the aldehyde mode and exhibit stronger overall adsorption. The trade-off in mode also generally manifests at lower *d*-filling for the 4*d* and 5*d* guests. Understanding these effects and separating the specific influence of narrowed states from broader periodic trends requires examination of the electronic factors governing adsorption.

In a two-level interaction model (Figure 3A), orbital hybridization can be largely encapsulated in terms of the coupling strength (V) between states. The upward and downward shift of bonding and antibonding states due to hybridization (E_{hyb}) is roughly equal to $\pm|V|$ when states are near-resonant and approaches $\pm\left|\frac{V^2}{\varepsilon_i-\varepsilon_j}\right|$ as the energy separation becomes larger.[24,25] A penalty (approximately

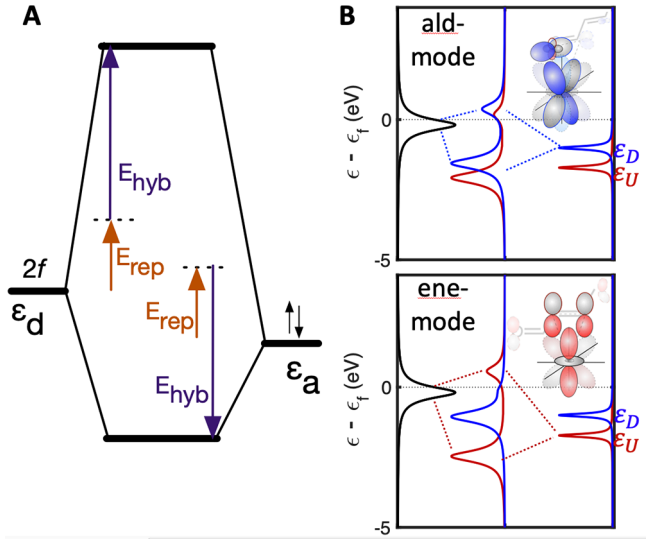

Figure 3. (A) Two-level interaction showing contributions of hybridization (E_{hyb}) and repulsion (E_{rep}). (B) Newns−Anderson−Grimley model for two-state selectivity. Initial adsorbate levels represent desired (ε_D, blue) and undesired (ε_U, red) states to activate. Tight binding parameters for each geometry using LCAO representations of the crotonaldehyde HOMO and HOMO−1 define the system.

proportional to V^2)[26,27] is also paid for reorthogonalization of overlapping states (Pauli repulsion, E_{rep}), resulting in the antibonding level being destabilized more than the bonding level is stabilized. For adsorption on *d*-metals these factors remain critical, but the energetic distribution of the states also merits consideration; this can be captured semiquantitatively within the Newns−Anderson−Grimley (NAG) model of chemisorption.[28−30] In the NAG framework, the distribution of the band, the initial adsorbate levels, and the coupling elements between them define the interaction. Exact parameters are not critical to the qualitative output, but for crotonaldehyde adsorption, we have considered the MOs as linear combinations of atomic orbitals (LCAO) and estimated coupling strengths between states with tabulated tight-binding relationships[31−33] (Figure S2 and SI Methods). Using these assumptions, Figure 3B shows representative model outputs

https://doi.org/10.1021/jacs.1c04234
J. Am. Chem. Soc. 2021, 143, 11897−11902

for the adsorbate pDOS on an SAA site in each relevant geometry. The NAG pDOS qualitatively resembles Figure 3A, but with bonding and antibonding bands associated with each orbital. The apparent asymmetry between bonding and antibonding can be understood in that the colored DOS features are projected on the adsorbate, and (for this example) the bonding levels have more adsorbate character, whereas the antibonding have more *d*-character. Adsorption energy differences also follow from the model (SI Methods).

Since hybridization requires both spatial and energetic overlap, the defining differences in adsorption energies come from comparing coupling to the HOMO while in the ald-mode against coupling to the HOMO−1 while in the ene-mode. In this comparison the coupling element is slightly larger for the HOMO due to shorter bond distance, but the interplay between resonance, Pauli repulsion, and occupation creates scenarios where either orbital interaction can be favored. To remove confounding factors and focus on the role of perturbation to the *d*-band, adsorbate geometries and coupling elements have been fixed to those on a reference surface (Co/Au) that was determined by DFT to show near-equal binding energies in both modes. Figure 4A shows resulting *differences* in *d*-band interaction energy ($\Delta\Delta E$) between each adsorption mode over a designated range of *d*-band center and width. Strong preference for the HOMO can be seen for high-lying, nearly empty *d*-states, which balance resonance with this higher energy MO against overcontributing electron density to antibonding states. This behavior for high *d*-band centers could only be inverted if the coupling element toward the HOMO−1 were much larger, to compensate for the better energy alignment of the HOMO and larger HOMO coupling element. The HOMO stabilization diminishes at very high band centers due to the growing energetic misalignment, and, more interestingly, is also diminished for similar reasons as the band becomes wider. The opposite selectivity is seen for low-lying, nearly filled *d*-states, which prefer the HOMO−1. While there is again a favorable contribution from resonance, the dominant factor is—perhaps counterintuitively—the smaller coupling element of the HOMO−1. The nearly filled surface *d*-orbitals of low bands yield high occupation of antibonding states, and while these antibonding states weaken interactions for both MOs, larger coupling toward the HOMO causes its associated Pauli repulsion (scaling as V^2) to be particularly unfavorable. This is, in general, the mechanism by which a weak-coupling interior orbital can be selected. The trends again remain magnified for narrower bands.

Several monometallic and SAA compositions are marked for illustration of broad trends in Figure 4A. However, for more quantitative agreement it is necessary to also account for periodic changes in coupling strength—multiple SAAs can have similar *d*-band centers and widths, but elements with larger spatial extents of *d*-orbitals will have stronger coupling to each MO (at a constant ratio, still preserving trends). The full parameter space of accessible SAA *d*-band characteristics is illustrated in Figure 4B, and period-specific (3*d*, 4*d*, 5*d*) selectivity maps (accounting for periodicity of *d*-orbital radii) are presented in Figure S5. Additional visualizations of the maps based on calculated DFT values are given in Figure S6. The period-resolved model is in good agreement with DFT, as seen in a parity plot in Figure 4B. Residual errors mainly stem from the approximation of fixed geometry (particularly in cases where absolute bond strength is very weak, such as on pure hosts) and from assignment of Lorentzian band shape to well-

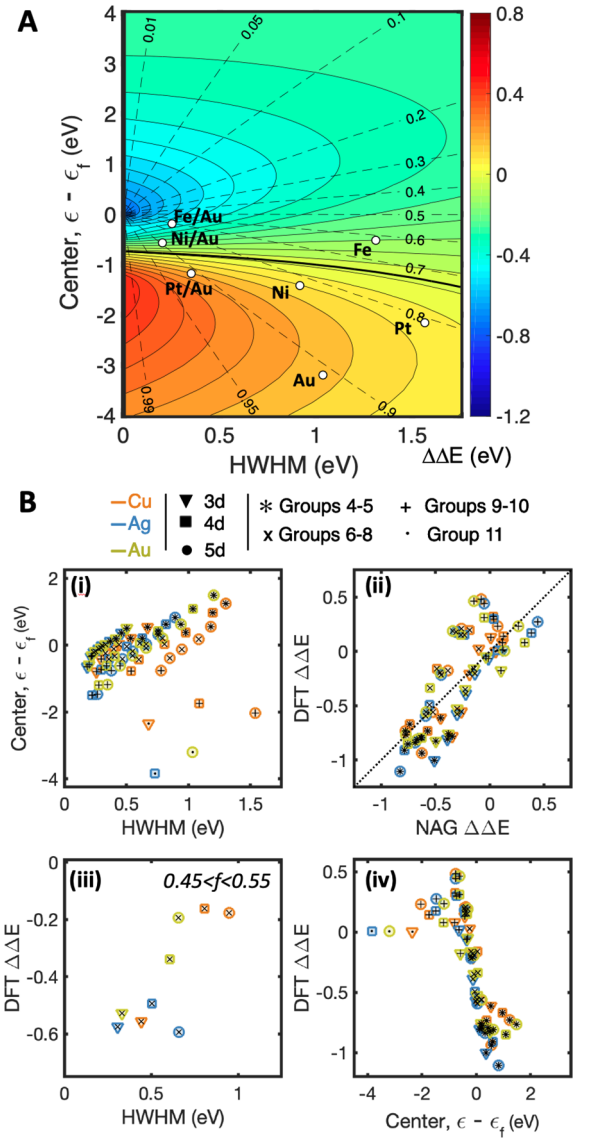

Figure 4. (A) Difference in *d*-band interaction between binding modes ($\Delta\Delta E = \Delta E_D^{ald} - \Delta E_U^{ene}$) vs band characteristics. Markers are only placed as a qualitative guide (cf. Figure S5 for period-specific selectivity maps). Dotted lines represent constant filling of a Lorentzian *d*-band. (B) Accessible parameter space of center and width (Lorentzian) for transition metal SAAs hosted in Cu, Ag, and Au (i); parity plot between period-adjusted NAG and DFT-calculated $\Delta\Delta E$ (ii); correlation of DFT $\Delta\Delta E$ with *d*-band width for intermediate fillings (iii); and correlation of DFT $\Delta\Delta E$ with *d*-band center (iv).

hybridized guests with large widths (cf. Figure S4). Figure 4B further shows correlations between the DFT $\Delta\Delta E$ and *d*-band center and width. While a stronger relationship with *d*-band center is clear (and noting center and width are correlated for constant *d*-state filling), the calculations nonetheless highlight a distinct role still played by broadening to weaken and distribute interactions toward both orbitals, dampening selectivity. This is isolated in the vicinity of $f \approx 0.5$.

To further illustrate the relationship between band narrowing and resonant interactions, Figure 5 compares the DFT-calculated orbital pDOS for adsorption of crotonaldehyde on monometallic Fe, Pt, and Au(111) to that when the respective Fe and Pt states become sharpened at isolated sites

https://doi.org/10.1021/jacs.1c04234
J. Am. Chem. Soc. 2021, 143, 11897−11902

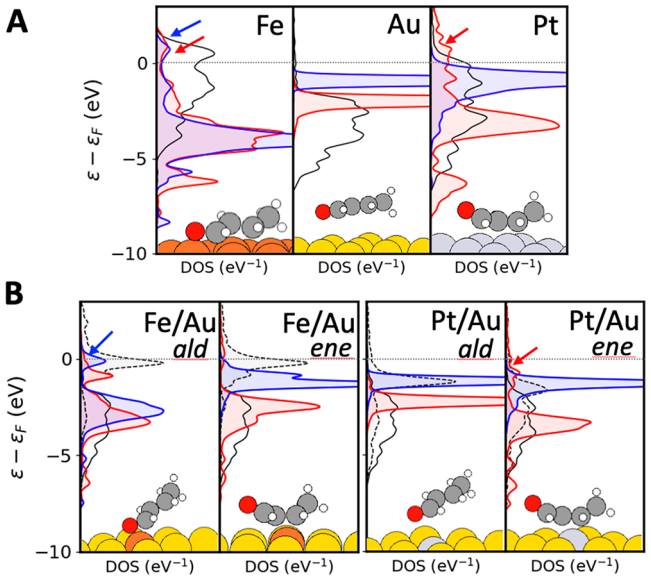

Figure 5. (A) Projected DOS for HOMO (blue) and HOMO−1 (red) of crotonaldehyde in its most stable adsorption geometry (insets) on monometallic Fe, Au, and Pt (111) surfaces. (B) Projected DOS for crotonaldehyde MOs adsorbed at isolated guest atom sites of Fe/Au ($\Delta\Delta E$ = −0.16) and Pt/Au ($\Delta\Delta E$ = +0.23) SAAs in both stable geometries (insets). In each panel the pDOS for host metal (solid black) and guest (dashed black, shaded) are also overlaid, and the arrows signify antibonding levels of activated bonds.

hosted within Au. In the case of monometallic Fe, the high energy center and breadth of *d*-states lead to hybridization with both functional groups (η_4 adsorption), with net bonding interactions indicated by partially depopulated antibonding states. While this simultaneous hybridization is also enabled by the geometry of contiguous Fe sites present, we can still contrast the orbital interactions with those found in each adsorption mode on the isolated Fe SAA. There, due to the higher *d*-center of isolated Fe, the ene-mode has a more asymmetric interaction, where the bonding level mainly has character of the former HOMO−1 and antibonding level has more Fe-character (recall the plots are projected on the adsorbate). In the ald-mode, however, the HOMO is better aligned with the sharpened Fe-state and experiences more effective hybridization than in the monometallic case. It may also be noted that the HOMO−1 still shows a hybridization pattern in the ald-mode—this is related to having some orbital density on the O atom and adds a small extra repulsive contribution (Figures S2−S3).

On Pt, the ene-mode of binding is preferred on both monometallic and single-atom sites, though it is weakened on the single atom. Upon state sharpening, the Pt *d*-band becomes positioned between the two critical MO's (cf. Figure 1), causing a similar degree of energetic overlap. This leads to spatial overlap effects dominating, and, combined with the high filling of the Pt states (promoting population of antibonding levels), leads to a dominant role of Pauli repulsion disfavoring the HOMO in the ald-mode. Additional guest elements within Cu, Ag, and Au hosts display similarly interpretable behaviors and are explored in Figures S7−S8.

To conclude, we have shown how local electronic structure of SAA surface sites can be chosen to promote interaction with specific molecular orbitals. The approach could broadly be applied to intramolecular chemo- or regioselectivity problems, or selectivity in mixtures, as long as key MOs are spatially localized (Figures S9−S10). We also note that, for brevity, we have neglected a number of important considerations for the suggested selectivity principle. Adsorption is but one step in a catalytic cycle; though it may tip selectivity toward a given route, all down-pathway intermediates must be considered. Figures S11−S12 show full reaction path free-energy diagrams for formation of both crotyl alcohol and butanal on Au, Fe/Au, and Pt/Au surfaces, as well as their MO diagrams. In each case, the favored route to product on the guest site is consistent with the initial adsorption mode. While experimental validation of selectivity trends on monometallics[34−37] and traditional alloys[38−40] are plentiful, we are only aware of one example using an SAA.[41] This involved acrolein hydrogenation on Pd/Ag, where the isolated site and host have competing reactivity (similar to Pt/Au here). A general design principle may be that guest sites should complement or have much higher intrinsic rates than host sites. We further acknowledge that in some cases materials may prefer surface segregation of the host element;[42] however, surface termination will be a function of the reactive environment, as has been shown for several SAAs.[43] Ultimately, SAAs will likely not provide a universal solution to selectivity problems, but they represent a possible new paradigm for selectivity control by expanding the available palette of electronic characteristics for tuning catalysis.

■ ASSOCIATED CONTENT

Supporting Information

The Supporting Information is available free of charge at https://pubs.acs.org/doi/10.1021/jacs.1c04234.

Full computational methods; periodic trends in *d*-band characteristics of SAAs and *d*-DOS plots for selected SAAs; LCAO states for crotonaldehyde; orbital-wise energy contributions and selectivity diagrams for alternate *d*-band shapes; selectivity model with period and filling dependent coupling elements; orbital pDOS for each adsorption geometry across selected SAAs; free energy diagrams for full reaction pathways on representative SAAs; MOs of down-pathway intermediates and other α,β-unsaturated aldehydes; visualization of orbital shifts near resonance and model outputs for differing MO separations; coupling matrix elements for orbitals with variable orientation to the surface (PDF)

■ AUTHOR INFORMATION

Corresponding Author

Adam Holewinski − *Department of Chemical and Biological Engineering, University of Colorado, Boulder, Colorado 80303, United States; Renewable and Sustainable Energy Institute, University of Colorado, Boulder, Colorado 80303, United States;* orcid.org/0000-0001-8307-5881; Email: adam.holewinski@colorado.edu

Author

Taylor D. Spivey − *Department of Chemical and Biological Engineering, University of Colorado, Boulder, Colorado 80303, United States; Renewable and Sustainable Energy Institute, University of Colorado, Boulder, Colorado 80303, United States*

Complete contact information is available at: https://pubs.acs.org/10.1021/jacs.1c04234

Notes

The authors declare no competing financial interest.

■ ACKNOWLEDGMENTS

The authors acknowledge funding support from the National Science Foundation (CBET 1944834). TDS acknowledges partial support from the Graduate Assistance in Areas of National Need (GAANN) fellowship from the U.S. Department of Education and partial support from the U.S. Department of Energy, Office of Science, Office of Workforce Development for Teachers and Scientists, Office of Science Graduate Student Research (SCGSR) program. The SCGSR program is administered by the Oak Ridge Institute for Science and Education (ORISE) for the DOE. ORISE is managed by ORAU under contract number DE-SC0014664. All opinions expressed in this paper are the authors' and do not necessarily reflect the policies and views of DOE, ORAU, or ORISE. This work utilized the RMACC Summit supercomputer, which is supported by NSF awards ACI-1532235 and ACI-1532236, the University of Colorado Boulder, and Colorado State University. The Summit supercomputer is a joint effort of the University of Colorado Boulder and Colorado State University. The authors would also like to thank Hongliang Xin for helpful discussion of modeling and Phillip Christopher for a thoughtful reading of the manuscript.

■ REFERENCES

(1) Kahsar, K. R.; Schwartz, D. K.; Medlin, J. W. Control of metal catalyst selectivity through specific noncovalent molecular interactions. *J. Am. Chem. Soc.* **2014**, *136*, 520−526.

(2) Dinh, K. T.; Sullivan, M. M.; Narsimhan, K.; Serna, P.; Meyer, R. J.; Dincă, M.; Román-Leshkov, Y. Continuous Partial Oxidation of Methane to Methanol Catalyzed by Diffusion-Paired Copper Dimers in Copper-Exchanged Zeolites. *J. Am. Chem. Soc.* **2019**, *141*, 11641−11650.

(3) Hammer, B. Special sites at noble and late transition metal catalysts. *Top. Catal.* **2006**, *37*, 3−16.

(4) Christensen, C. H.; Norskov, J. K. A molecular view of heterogeneous catalysis. *J. Chem. Phys.* **2008**, *128*, 182503.

(5) Thirumalai, H.; Kitchin, J. R. Investigating the Reactivity of Single Atom Alloys Using Density Functional Theory. *Top. Catal.* **2018**, *61*, 462−474.

(6) Greiner, M. T.; Jones, T. E.; Beeg, S.; Zwiener, L.; Scherzer, M.; Girgsdies, F.; Piccinin, S.; Armbrüster, M.; Knop-Gericke, A.; Schlögl, R. Free-atom-like d states in single-atom alloy catalysts. *Nat. Chem.* **2018**, *10*, 1008−1015.

(7) Enkovaara, J.; Rostgaard, C.; Mortensen, J. J.; Chen, J.; Dułak, M.; Ferrighi, L.; Gavnholt, J.; Glinsvad, C.; Haikola, V.; Hansen, H. A.; Kristoffersen, H. H.; Kuisma, M.; Larsen, A. H.; Lehtovaara, L.; Ljungberg, M.; Lopez-Acevedo, O.; Moses, P. G.; Ojanen, J.; Olsen, T.; et al. Electronic structure calculations with GPAW: A real-space implementation of the projector augmented-wave method. *J. Phys.: Condens. Matter* **2010**, *22*, 253202.

(8) Mortensen, J. J.; Hansen, L. B.; Jacobsen, K. W. Real-space grid implementation of the projector augmented wave method. *Phys. Rev. B: Condens. Matter Mater. Phys.* **2005**, *71*, 1−11.

(9) Darby, M. T.; Stamatakis, M.; Michaelides, A.; Sykes, E. C. H. Lonely Atoms with Special Gifts: Breaking Linear Scaling Relationships in Heterogeneous Catalysis with Single-Atom Alloys. *J. Phys. Chem. Lett.* **2018**, *9*, 5636−5646.

(10) Giannakakis, G.; Flytzani-Stephanopoulos, M.; Sykes, E. C. H. Single-Atom Alloys as a Reductionist Approach to the Rational Design of Heterogeneous Catalysts. *Acc. Chem. Res.* **2019**, *52*, 237−247.

(11) Darby, M. T.; Réocreux, R.; Sykes, E. C. H.; Michaelides, A.; Stamatakis, M. Elucidating the Stability and Reactivity of Surface Intermediates on Single-Atom Alloy Catalysts. *ACS Catal.* **2018**, *8*, 5038−5050.

(12) Lucci, F. R.; Marcinkowski, M. D.; Lawton, T. J.; Sykes, E. C. H. H2 Activation and Spillover on Catalytically Relevant Pt-Cu Single Atom Alloys. *J. Phys. Chem. C* **2015**, *119*, 24351−24357.

(13) Kyriakou, G.; Boucher, M. B.; Jewell, A. D.; Lewis, E. A.; Lawton, T. J.; Baber, A. E.; Tierney, H. L.; Flytzani-Stephanopoulos, M.; Sykes, E. C. H. Isolated metal atom geometries as a strategy for selective heterogeneous hydrogenations. *Science* **2012**, *335*, 1209−1212.

(14) Boucher, M. B.; Zugic, B.; Cladaras, G.; Kammert, J.; Marcinkowski, M. D.; Lawton, T. J.; Sykes, E. C. H.; Flytzani-Stephanopoulos, M. Single atom alloy surface analogs in Pd0.18Cu15 nanoparticles for selective hydrogenation reactions. *Phys. Chem. Chem. Phys.* **2013**, *15*, 12187−12196.

(15) Cao, X.; Mirjalili, A.; Wheeler, J.; Xie, W.; Jang, B. W. L. Investigation of the preparation methodologies of Pd-Cu single atom alloy catalysts for selective hydrogenation of acetylene. *Front. Chem. Sci. Eng.* **2015**, *9*, 442−449.

(16) Liu, J.; Shan, J.; Lucci, F. R.; Cao, S.; Sykes, E. C. H.; Flytzani-Stephanopoulos, M. Palladium-gold single atom alloy catalysts for liquid phase selective hydrogenation of 1-hexyne. *Catal. Sci. Technol.* **2017**, *7*, 4276−4284.

(17) Lucci, F. R.; Liu, J.; Marcinkowski, M. D.; Yang, M.; Allard, L. F.; Flytzani-Stephanopoulos, M.; Sykes, E. C. H. Selective hydrogenation of 1,3-butadiene on platinum-copper alloys at the single-atom limit. *Nat. Commun.* **2015**, *6*, 1−8.

(18) Fung, V.; Hu, G.; Sumpter, B. Electronic band contraction induced low temperature methane activation on metal alloys. *J. Mater. Chem. A* **2020**, *8*, 6057−6066.

(19) Hammer, B.; Nørskov, J.K. Electronic factors determining the reactivity of metal surfaces. *Surf. Sci.* **1995**, *343*, 211−220.

(20) Hammer, B.; Norskov, J. K. Theoretical surface science and catalysis–calculations and concepts. *Adv. Catal.* **2000**, *45*, 71−129.

(21) Luneau, M.; Lim, J. S.; Patel, D. A.; Sykes, E. C. H.; Friend, C. M.; Sautet, P. Guidelines to Achieving High Selectivity for the Hydrogenation of α,β-Unsaturated Aldehydes with Bimetallic and Dilute Alloy Catalysts: A Review. *Chem. Rev.* **2020**, *120*, 12834−12872.

(22) Liu, W.; Jiang, Y.; Dostert, K.-H.; O'Brien, C. P.; Riedel, W.; Savara, A.; Schauermann, S.; Tkatchenko, A. Catalysis beyond frontier molecular orbitals: Selectivity in partial hydrogenation of multi-unsaturated hydrocarbons on metal catalysts. *Sci. Adv.* **2017**, *3*, No. e1700939.

(23) Haubrich, J.; Loffreda, D.; Delbecq, F.; Sautet, P.; Krupski, A.; Becker, C.; Wandelt, K. Adsorption of α,β-Unsaturated Aldehydes on Pt (111) and Pt - Sn Alloys : II. Crotonaldehyde. *J. Phys. Chem. C* **2009**, *113*, 13947−13967.

(24) Atkins, P.; de Paula, J. *Physical Chemistry: Thermodynamics, Structure, and Change*; Oxford University Press, 2014; pp 399−435.

(25) Chorkendorff, I.; Niemantsverdriet, J. *Concepts of Modern Catalysis and Kinetics*; Wiley-VCH, 2003; pp 215−266.

(26) Hammer, B.; Morikawa, Y.; Norskov, J. K. CO chemisorption at metal surfaces and overlayers. *Phys. Rev. Lett.* **1996**, *76*, 2141−2144.

(27) Wang, S.; Pillai, H. S.; Xin, H. Bayesian learning of chemisorption for bridging the complexity of electronic descriptors. *Nat. Commun.* **2020**, *11*, 1−7.

(28) Newns, D. M. Self-consistent model of hydrogen chemisorption. *Phys. Rev.* **1969**, *178*, 1123−1135.

(29) Muscat, J. P.; Newns, D. M. Chemisorption on metals. *Prog. Surf. Sci.* **1978**, *9*, 1−43.

(30) Grimley, T. B. Chemisorption Theory. *Prog. Surf. Membr. Sci.* **1975**, *9*, 71−161.

(31) Harrison, W. A. *Electronic Structure and the Properties of Solids: The Physics of the Chemical Bond*; Dover Publications, 1989; p 552.

(32) Slater, J. C.; Koster, G. F. Simplified LCAO method for the periodic potential problem. *Phys. Rev.* **1954**, *94*, 1498−1524.

https://doi.org/10.1021/jacs.1c04234
J. Am. Chem. Soc. 2021, 143, 11897−11902

(33) Nørskov, J. K. Effective medium potentials for molecule-surface interactions: H2 on Cu and Ni surfaces. *J. Chem. Phys.* **1989**, *90*, 7461−7471.
(34) Zanella, R.; Louis, C.; Giorgio, S.; Touroude, R. Crotonaldehyde hydrogenation by gold supported on TiO2: Structure sensitivity and mechanism. *J. Catal.* **2004**, *223*, 328−339.
(35) Wei, H.; Gomez, C.; Liu, J.; Guo, N.; Wu, T.; Lobo-Lapidus, R.; Marshall, C. L.; Miller, J. T.; Meyer, R. J. Selective hydrogenation of acrolein on supported silver catalysts: A kinetics study of particle size effects. *J. Catal.* **2013**, *298*, 18−26.
(36) Marinelli, T. B. L. W.; Ponec, V. A study on the selectivity in acrolein hydrogenation on platinum catalysts: A model for hydrogenation of α,β-unsaturated aldehydes. *J. Catal.* **1995**, *156*, 51−59.
(37) Mohr, C.; Hofmeister, H.; Radnik, J.; Claus, P. Identification of active sites in gold-catalyzed hydrogenation of acrolein. *J. Am. Chem. Soc.* **2003**, *125*, 1905−1911.
(38) Gyorffy, N.; Paál, Z. Acrolein hydrogenation on PdPt powder catalysts prepared by colloid synthesis. *J. Mol. Catal. A: Chem.* **2008**, *295*, 24−28.
(39) Murillo, L. E.; Goda, A. M.; Chen, J. G. Selective hydrogenation of the C = O bond in acrolein through the architecture of bimetallic surface structures. *J. Am. Chem. Soc.* **2007**, *129*, 7101−7105.
(40) Haass, F.; Bron, M.; Fuess, H.; Claus, P. In situ X-ray investigations on AgIn/SiO2 hydrogenation catalysts. *Appl. Catal., A* **2007**, *318*, 9−16.
(41) Aich, P.; Wei, H.; Basan, B.; Kropf, A. J.; Schweitzer, N. M.; Marshall, C. L.; Miller, J. T.; Meyer, R. Single-Atom Alloy Pd-Ag Catalyst for Selective Hydrogenation of Acrolein. *J. Phys. Chem. C* **2015**, *119*, 18140−18148.
(42) Rao, K. K.; Do, Q. K.; Pham, K.; Maiti, D.; Grabow, L. C. Extendable Machine Learning Model for the Stability of Single Atom Alloys. *Top. Catal.* **2020**, *63*, 728−741.
(43) Darby, M. T.; Sykes, E. C. H.; Michaelides, A.; Stamatakis, M. Carbon Monoxide Poisoning Resistance and Structural Stability of Single Atom Alloys. *Top. Catal.* **2018**, *61*, 428−438.

https://doi.org/10.1021/jacs.1c04234
J. Am. Chem. Soc. 2021, 143, 11897−11902